A numerical study of the Magellan Plume

Elbio D. Palma[1] and Ricardo P. Matano[2]

Received 10 November 2011; revised 16 April 2012; accepted 16 April 2012; published 26 May 2012.

[1] In this modeling study we investigate the dynamical mechanisms controlling the spreading of the Magellan Plume, which is a low-salinity tongue that extends along the Patagonian Shelf. Our results indicate that the overall characteristics of the plume (width, depth, spreading rate, etc.) are primarily influenced by tidal forcing, which manifests through tidal mixing and tidal residual currents. Tidal forcing produces a homogenization of the plume's waters and an offshore displacement of its salinity front. The interaction between tidal and wind-forcing reinforces the downstream and upstream buoyancy transports of the plume. The influence of the Malvinas Current on the Magellan Plume is more dominant north of 50°S, where it increases the along-shelf velocities and generates intrusions of saltier waters from the outer shelf, thus causing a reduction of the downstream buoyancy transport. Our experiments also indicate that the northern limit of the Magellan Plume is set by a high salinity discharge from the San Matias Gulf. Sensitivity experiments show that increments of the wind stress cause a decrease of the downstream buoyancy transport and an increase of the upstream buoyancy transport. Variations of the magnitude of the discharge produce substantial modifications in the downstream penetration of the plume and buoyancy transport. The Magellan discharge generates a northeastward current in the middle shelf, a recirculation gyre south of the inlet and a region of weak currents father north.

Citation: Palma, E. D., and R. P. Matano (2012), A numerical study of the Magellan Plume, *J. Geophys. Res.*, *117*, C05041, doi:10.1029/2011JC007750.

1. Introduction

[2] The Magellan Plume (MP hereafter) is a tongue of low-salinity waters that extends along the Patagonian Shelf from approximately 54°S to 42°S (Figure 1). This plume is formed by the discharge of relatively fresh waters from the Magellan Strait, which is a narrow and winding passage that connects the Pacific and Atlantic shelves of South America, and by small contributions from local rivers [*Pasquini and De Petris*, 2007].

[3] The limits of the MP, defined by the 33.5 isohaline, extend both downstream and upstream of the Magellan Strait [*Bianchi et al.*, 2005]. The downstream extension flows close to the coast until it reaches 47°S, where it moves offshore toward the middle shelf and continues its northward trajectory until approximately 42°S (Figure 1). The MP extends from the surface to the bottom (Figures 1b and 1c). This type of plume has been called "bottom advected" because its spreading appeared to be controlled by advection in the bottom boundary layer [*Chapman and Lentz*, 1994; *Yankovsky and Chapman*, 1997]. *Matano and Palma* [2010a], however, argued that it should be called "bottom trapped" because the downstream spreading is not driven by bottom boundary layer processes but by the barotropic pressure gradient; that is, the plume will flow downstream even if there were no bottom boundary layer. The offshore scale of the MP is ∼300 km, and the vertical scale (i.e., maximum depth attained) is ∼120 m (Figures 1b and 1c).

[4] *Brandhorst and Castello* [1971] speculated that associated with the MP there could be a northeastward current that they called the Patagonian Current. There are no current meter observations to confirm this hypothesis, but numerical simulations show an increase of the mid-shelf velocities that is coincidental with the path of the MP [*Palma et al.*, 2008]. The dynamical mechanisms controlling the path and volume transport of this current remain uncertain. These matters are important because this region is one of the most productive portions of the Patagonian Shelf. Satellite images, for example, indicate that the Magellan Strait discharge might be an important source of nutrients for the remarkable chlorophyll blooms that characterize this region [*Romero et al.*, 2006].

[5] In this article we seek to establish the dynamical mechanisms that control the spreading of the MP. In particular, we aim to elucidate the role of tides, winds and the influence of the local western boundary current, the Malvinas Current, on the plume structure. Some of the questions we would like to answer include: What controls the along- and cross-shelf penetration as well as the vertical stratification of

[1]Departamento de Fisica and Instituto Argentino de Oceanografía, CONICET, Universidad Nacional del Sur, Bahia Blanca, Argentina.
[2]College of Earth, Ocean, and Atmospheric Sciences, Oregon State University, Corvallis, Oregon, USA.

Corresponding author: E. D. Palma, Departamento de Fisica, Universidad Nacional del Sur, Av. Alem 1253, Bahia Blanca, Buenos Aires 8000, Argentina. (uspalma@criba.edu.ar)

0148-0227/12/2011JC007750

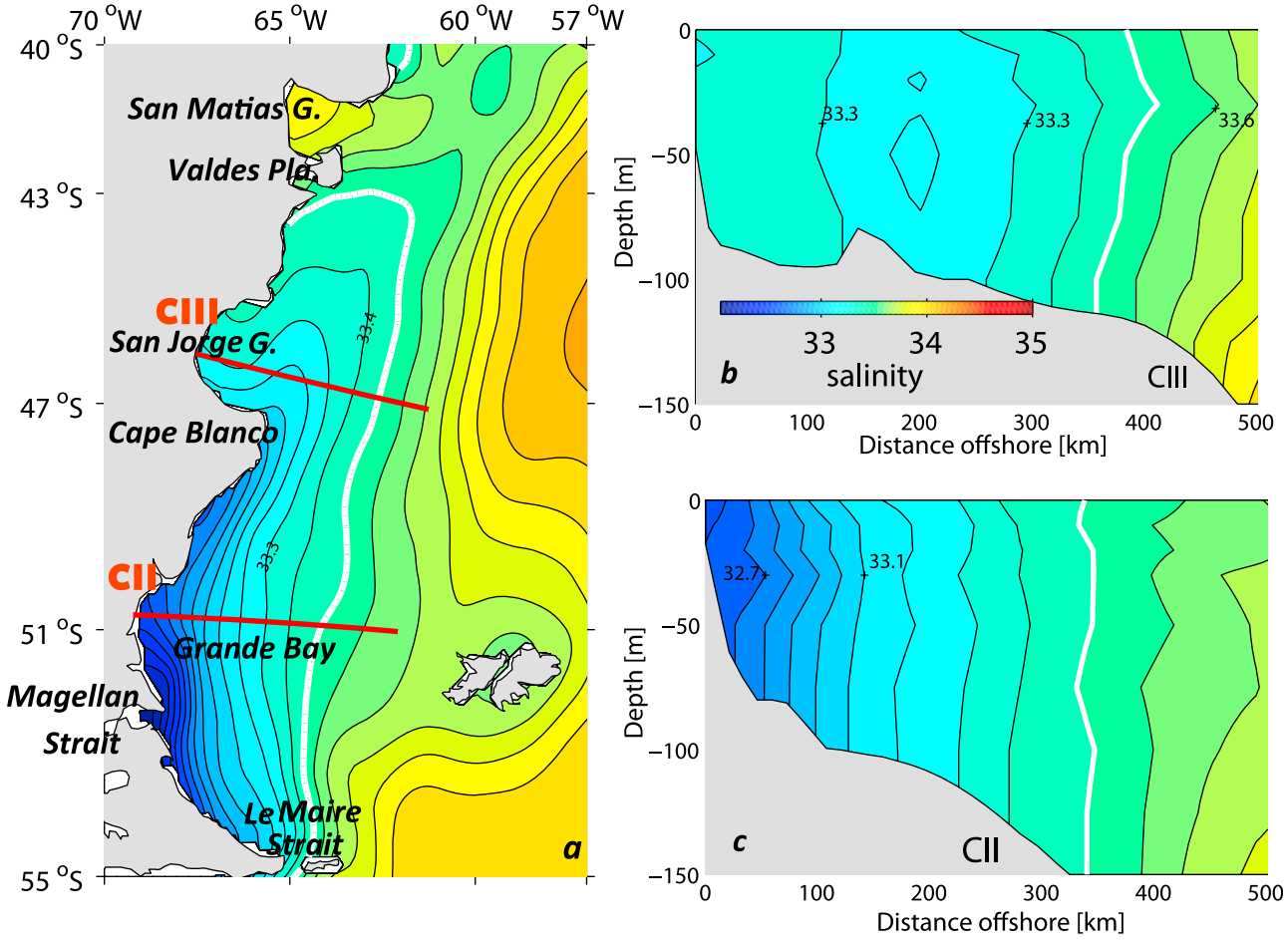

Figure 1. (a) Sea surface salinity in the Patagonian Shelf from climatologically averaged hydrographic observations. (b and c) Climatological cross-sections of salinity at sections CIII and CII. The white line indicates the position of the 33.5 isohaline.

the plume? Why does the plume detach from the coast north of 47°S? Additionally we seek to determine the influence of this plume on the Patagonian Shelf circulation and buoyancy transport.

2. Background Information

[6] The oceanic circulation over the Patagonian Shelf is driven by winds, tides and the offshore influence of the Malvinas Current (MC). The annual mean wind stress distribution over this region is characterized by a band of strong westerlies, which intensify during the austral winter (see *Palma et al.* [2004a] for a characterization of the wind-forcing and its impact on the shelf circulation). The tidal cycle is dominated by the semidiurnal component, which enters the Patagonian Shelf through its southern boundary and propagates northeastward as a Kelvin wave. Tidal amplitudes reach more than 4 m in Grande Bay and decrease sharply toward the north (0.25 m north of 35°S). Most of the tidal dissipation occurs in Grande Bay (south of 52°S) and near the Valdés Península (~41°S) [*Palma et al.*, 2004b]. The MC is a swift, barotropic, and narrow branch of the Antarctic Circumpolar Current that flows north along the continental slope of Argentina to nearly 38°S with a volume transport of approximately 40 Sv [*Vivier and Provost*, 1999]. Previous studies indicate that the MC has a strong influence on the shelf circulation [*Palma et al.*, 2008; *Piola et al.*, 2010; *Matano et al.*, 2010].

3. Model Description

[7] The numerical model used in this study is the Princeton Ocean Model [*Blumberg and Mellor*, 1987]. The model domain extends from 55°S to 18°S and from 70°W to 40°W with a horizontal grid resolution of 5 km near the western coast and 20 km near the eastern boundary. The model bathymetry was interpolated from the *Smith and Sandwell* [1997] data set. The vertical resolution of the model comprises 25 vertical sigma levels with higher resolution in the top and bottom boundary layers. Vertical mixing is parameterized with a 2.5 turbulent closure scheme [*Mellor and Yamada*, 1982; *Galperin et al.*, 1988]. Horizontal mixing is parameterized using a Smagorinsky scheme [*Smagorinsky*, 1963]. The advection of tracer fields is represented with a recursive Smolarkiewicz [*Smolarkiewicz and Grabowski*, 1990] scheme. The model has three open boundaries were a combination of radiation and advection boundary conditions are used [*Palma et al.*, 2008]. Tidal amplitudes and phases are

Table 1. Characteristics of the Numerical Experiments Described in the Text

Experiment	Initial Stratification	Q_o (m^3/s)	ΔS	Forcing	San Matias G. Relaxation
EXP1	S = 33.7	0.0	0.0	Tides	No
EXP2	"	"	"	Winds	No
EXP3	"	85,000	"	No	No
EXP4	"	"	−1.4	No	No
EXP5	"	"	"	Winds	No
EXP6	"	"	"	Tides	No
EXP7	"	"	"	Tides and Winds	No
EXP8	Ocean Atlas	"	"	Tides, Winds and MC	No
EXP9	"	"	"	"	Yes
EXP10	"	"	"	Tides, 2xWinds and MC	Yes
EXP11	"	"	"	Tides, 0.5xWinds and MC	Yes
EXP12	"	170,000	"	Tides, winds and MC	Yes
EXP13	"	42,500	−1.4	"	Yes
EXP14	"	0.0	0.0	"	Yes

interpolated form the *Egbert et al.* [1994] model, and boundary inflows are derived from the POCM-4 eddy-permitting global ocean model [*Tokmakian and Challenor*, 1999]. Wind stress forcing is derived from the QuikSCAT climatology [*Risien and Chelton*, 2008]. *Palma et al.* [2008] have shown that the mean circulation patterns produced by this model compares well with in situ and remote observations.

[8] To represent the Magellan Strait's discharge we use the numerical scheme designed by *Kourafalou et al.* [1996]. Water of prescribed salinity is introduced uniformly throughout the top half of the water column in the grid cells that represent the Strait's mouth. There are no in situ measurements of the magnitude of the Magellan's discharge; the value used in this study (Qo = 85,000 m^3/s) was estimated from a model of the strait that includes realistic coastlines, and bottom topography and salinity estimated from hydrographic measurements [*Panella et al.*, 1991], and was forced by westerly winds, tides and the mean sea level difference between the Pacific and Atlantic Ocean entrances [*Sassi and Palma*, 2006].

[9] To investigate the influence of external forcing on the MP we conducted four sets of numerical experiments, each designed to highlight a specific dynamical process (Table 1). The first set is focused on purely barotropic processes, i.e., with no density variations, and includes experiments forced by tides (EXP1), winds (EXP2) and a barotropic discharge from the Magellan Strait (EXP3). The second set of experiments investigates the dynamics of a low-salinity discharge onto a quiescent, non-stratified ocean (S = 33.7) with: (a) no external forcing (EXP4), (b) wind-forcing (EXP5), (c) tidal forcing (EXP6), and (d) the combined effect of tidal and wind-forcing (EXP7). The third set of experiments is set in a stratified ocean in which the salinity signature of the MP is removed from the initial conditions. This set of experiments is designed to test the influence of the Malvinas Current (EXP8) and the high-salinity discharge from San Matías Gulf (EXP9) onto the plume development. The fourth set of experiments (EXP10 to EXP14) investigates the sensitivity of the plume to the magnitude of the discharge, the buoyancy inflow and the magnitude of the wind stress forcing. The barotropic experiments were run for two years, the baroclinic experiments for six years. Our analysis focuses on the last year of the simulations. Table 1 summarizes the characteristics of the numerical experiments discussed in this article.

4. Results

4.1. Barotropic Experiments

[10] This set of experiments investigates the spreading of a discharge when density effects are neglected, i.e., when the density of the discharge is identical to the density of the interior of the basin. The spreading of the plume, therefore, is entirely driven by barotropic processes. The first two experiments do not include a discharge and are included to illustrate the potential contributions of tidal and wind-forcing to the plume development. EXP1 (Table 1), which is forced with tides only, shows the structure of the mean residual tidal current when there is no discharge from the Strait. Similar results are described in detail in *Palma et al.* [2004b], therefore only a brief synopsis is presented here. The tidal residual mean circulation consists of a broad anticyclonic gyre extending from 51°S to 42°S (Figure 2a). The left branch of the gyre flows southward following the coastal geometry and intensifies south of Cape Blanco. The right branch flows northward in the outer shelf between the 100 and 200 m isobaths. The larger currents (>15 cm/s) are found to the north of Valdés Peninsula and to the south of the Magellan Strait, where they form a dipole structure with closed gyres of opposite rotation. These gyres are generated by the nonlinear advection of residual vorticity generated by differential bottom friction [*Robinson*, 1983; *Ridderinkhof*, 1989]. There are scant in situ observations but the M_2 currents predicted by the model are in general agreement with those determined from current meter observations. The model also predicts correctly the location of the main frontal systems of the Patagonian Shelf region [*Palma et al.*, 2004b].

[11] EXP2 is forced with climatological winds (Table 1). The annual-mean circulation pattern is characterized by a broad, northeastward flow that intensifies toward the outer shelf (Figure 2b). Near 42°S a branch of this flow is diverted onshore, where it joins a southward coastal current that reaches up to the southern tip of Tierra del Fuego. Coastline indentations (e.g., the Grande Bay and the San Jorge Gulf) lead to the formation of anticyclonic, recirculating gyres with intense coastal currents. The middle and outer shelf

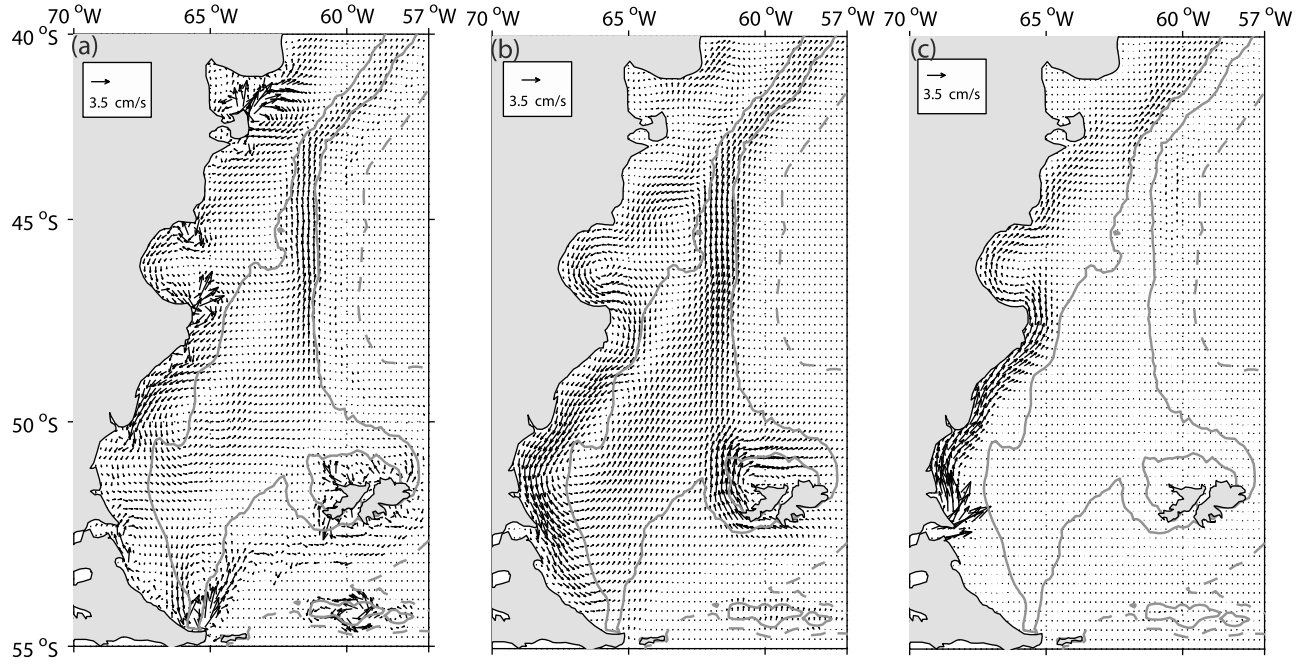

Figure 2. Depth-averaged annual mean barotropic circulation in the Patagonian Shelf for the experiments forced with (a) tides (EXP1), (b) climatological winds (EXP2) and (c) Magellan discharge (EXP3). The full gray lines indicate the 100 and 200 m isobaths. The gray dashed line indicates the 1000 m isobath.

equatorward currents are mostly driven by Ekman dynamics while the poleward coastal boundary current is associated with a wind-driven sea level set-down [*Palma et al.*, 2004b].

[12] EXP3 is forced with a discharge that has the same density than the basin. This experiment shows a relatively narrow coastal current flowing in the direction of the coastally trapped waves (the downstream direction). The downstream spreading of this current is in agreement with what is expected from the arrested topographic wave theory (Figure 2c) [*Csanady*, 1978].

4.2. Baroclinic Experiments Without External Forcing

[13] These experiments are forced with a buoyant inflow that has a volume discharge Q_o = 85,000 m^3/s and a salinity anomaly computed from historical hydrographic data $\Delta S = -1.4$ (negative salinity anomalies imply lighter waters) into a non-stratified shelf with no other external forcing (EXP4, Table 1). These values were chosen to mimic the conditions in the real ocean. In the following discussion the limits of the MP waters will be marked by the 33.5 isohaline. We choose a definition of the MP limits based on a particular isohaline instead of a salinity gradient because some of the experiments to be discussed do not always show a well-defined salinity front. Thus, in those experiments there is a gradual transition from fresher to saltier waters.

[14] The buoyant discharge generates a bottom-trapped plume in the inner shelf (up to ~50 km from the coast), and a mixed type plume farther offshore (Figures 3b and 3c). In contrast with the barotropic experiment (EXP3), a portion of the discharge now spreads in the upstream direction (Figure 3a). The Hovmöller diagram of the along-shelf surface salinity minimum shows an abrupt change of the spreading rate, from ~35 km/month to ~25 km/month, near 47°S (Figure 4a). Ancillary experiments (not shown) indicate that this change is associated with the flattening of the bottom slope in the northward region, which is reduced from a value of 5×10^{-4} to 1.5×10^{-4}. This result is consistent with previous studies showing that the rate of downstream spreading is proportional to the bottom slope [*Matano and Palma*, 2010a]. At the end of the six-year simulation the plume is located at 35°S and keeps spreading downstream. The plume shows downstream variations of its width, it is wider at the center of Grande Bay (~360 km), shrinks near Cape Blanco and expands again after 47°S (Figure 3a). According to *Chapman and Lentz* [1994] the cross-shelf spreading of a bottom-trapped plume is independent of the downstream location but it is otherwise inversely proportional to the slope of the bottom topography. The observed variations of the plume's width in the model results can therefore be ascribed to along-shelf changes in bottom slope. As noted above, the plume also spreads in the upstream direction albeit at a slower rate (Figure 4a). This behavior follows the development of a self-sustained baroclinic pressure gradient [*Matano and Palma*, 2010a, 2010b], and it has been documented in other regions of the world [e.g., *Piola et al.*, 2008; *Wu et al.*, 2011].

[15] To estimate the influence of the discharge on the salinity structure of the shelf we computed the along-shelf buoyancy anomaly transport (buoyancy transport hereafter) defined as

$$Q_b = \iint v \frac{\Delta S}{S_o} dxdz, \tag{1}$$

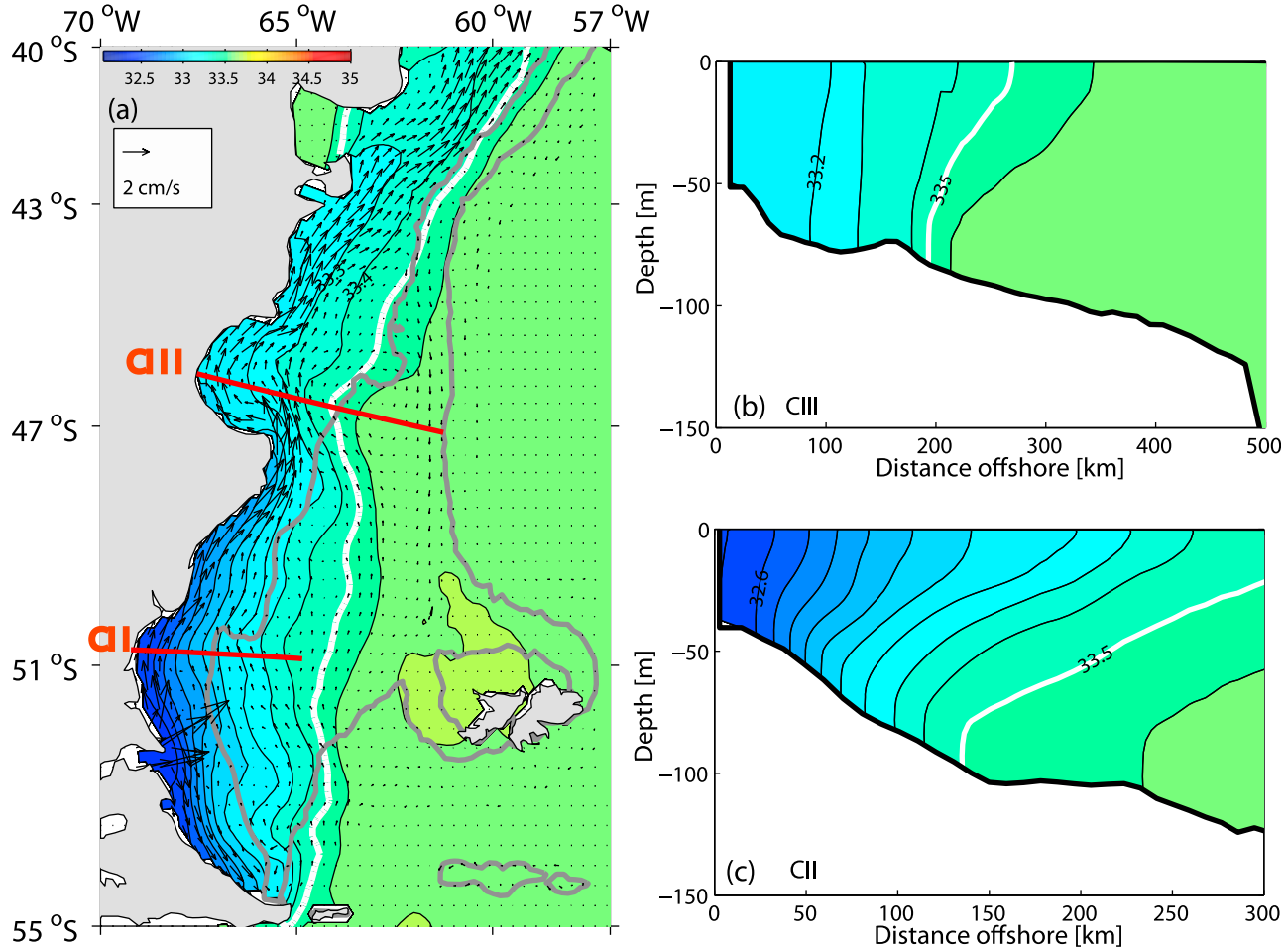

Figure 3. (a) Sea surface salinity and depth-averaged velocity vectors in the Patagonian Shelf from the experiment forced by the discharge only (EXP4). Grey lines indicate the 100 and 200 m isobaths. (b) Cross section of salinity at section CIII. (c) Same as Figure 3b but for section CII. The white line indicates the 33.5 isohaline.

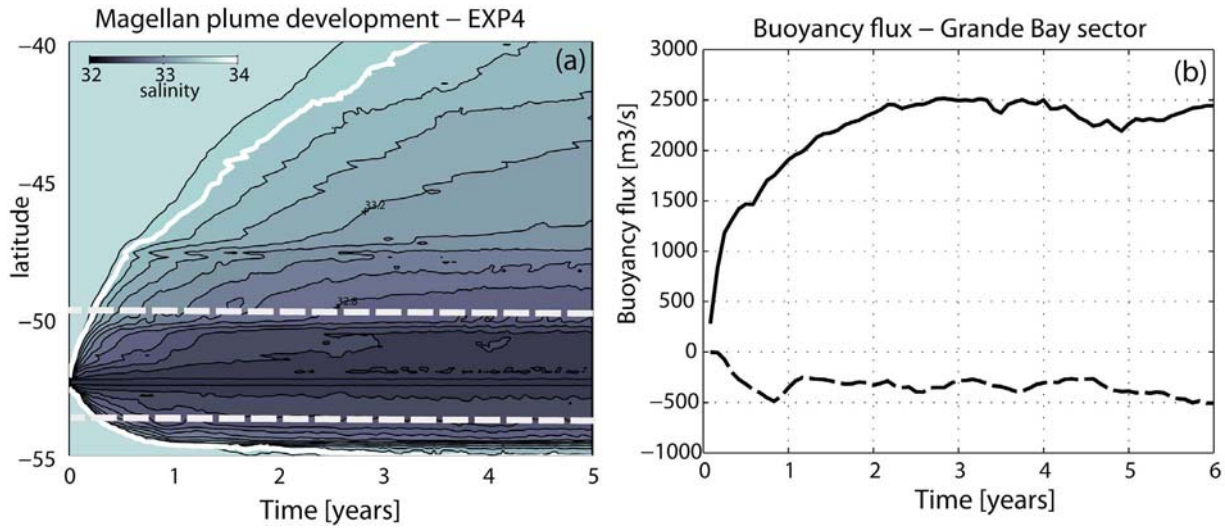

Figure 4. (a) Hovmöller diagram of sea surface salinity minimum along the Patagonian Shelf from the experiment forced by the discharge only. The white line is the 33.5 isohaline. (b) Time evolution of along-shelf buoyancy transport. Full line is for a cross-section to the north of Magellan Strait and the dashed line is for a southern cross-section (marked dashed in Figure 4a).

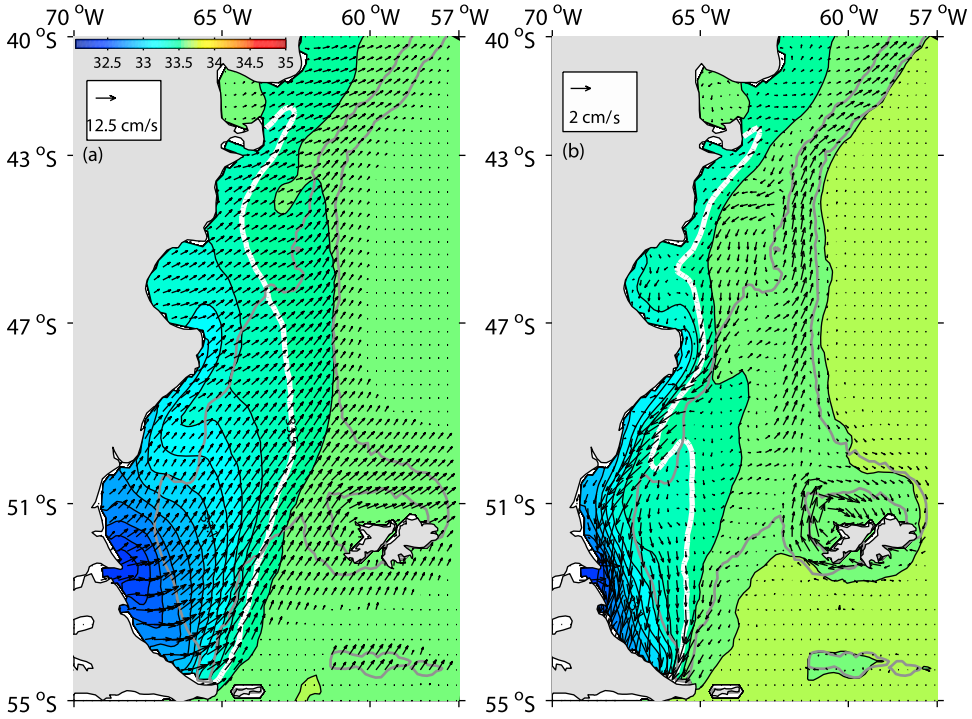

Figure 5. (a) Sea surface salinity and surface layer velocity vectors in the Patagonian Shelf from the experiment forced by the discharge and climatological winds (EXP5). (b) Bottom layer salinity and velocity vectors. The white line indicates the 33.5 isohaline. The gray lines indicate the 100 and 200 m isobaths.

where v is the along-shelf velocity, ΔS the salinity difference between the plume and ambient water (S_o = 33.7), and the integration is performed over a depth/cross-shore section (x, z) [*Fong and Geyer*, 2002]. In our experiment the discharge is 85,000 m^3/s, the salinity anomaly ΔS = 1.4, and the total buoyancy transport at the inlet is Q_{bi} = 3500 m^3/s. The buoyancy fluxes are computed at a downstream and at an upstream section (Figure 4a). After a spin-up period of approximately 3 years the buoyancy discharge is unevenly distributed, with a downstream buoyancy transport of ~2500 m^3/s and an upstream buoyancy transport of ~500 m^3/s (Figure 4b). *Matano and Palma* [2010a] show that the divergence of the discharge is associated with the geostrophic adjustment of the flow. Ancillary experiments indicate that the fraction of the buoyancy inflow diverted to the upstream and the downstream regions is proportional to the magnitude of the bottom slope with gentler slopes favoring the downstream transport and vice versa.

[16] EXP4 shows substantial differences with observations, the model's plume flows closer to the coast and it is more vertically stratified than the actual MP (e.g., Figure 1). These differences accentuate north of 47°S, where EXP4 shows a plume that remains trapped near the coast while the observations show that the plume detaches from the coast and moves toward the mid shelf. The causes of these differences will be discussed in the following sections.

4.3. Forced Baroclinic Experiments

[17] EXP5 adds a westerly wind-forcing to the EXP4 setup (Table 1). The annually averaged sea surface salinity distribution indicates that the wind stress forcing increases the offshore spreading of the plume and reduces its downstream penetration (Figure 5a). In the middle shelf the wind forces a circulation cell with lighter water flowing northeastward at the surface and denser water moving southwestward at the bottom (Figures 5a and 5b). This circulation pattern, which advects lighter waters onto the surface layers and denser waters onto the bottom layers, strengthens the vertical stratification and generates a surface intensified plume. The comparison of EXP5 with EXP4 indicates that that while the boundaries of the plume expand at the surface they contract at depth (Figure 6a). The wind-forcing also generates a deep coastal undercurrent (Figure 5b), and reduces the rate of downstream spreading (Figure 6b). The temporal evolution of the sea surface 33.5 isohaline shows a weak temporal oscillation that is associated with the seasonal variations of the wind-forcing. The inclusion of wind-forcing does not increase the realism of the simulation but reduces it.

[18] EXP6 adds tidal forcing to the EXP4 setup (Table 1). Tidal induced mixing produces a substantial homogenization of the water column and sharpens the cross-shelf salinity gradients (Figures 7a and 7b). The enhancement of the vertical mixing increases the salinity of the upper layers and decreases the salinity of the bottom layers causing the contraction of the plume's limit at the surface and its expansion at the bottom (compared with EXP4 and EXP5, Figure 6a). The downstream penetration of the plume and its spreading rate in EXP6 are similar to those of EXP5 (wind-forcing), but are smaller than those of EXP4 (unforced). The upstream spreading rate in EXP6 is substantially smaller than previous experiments (Figure 6b). More importantly, tidal forcing causes an offshore displacement of the salinity front (measured by the maximum salinity gradient) of approximately 100 km offshore at the Grande Bay (Figure 8b), which is

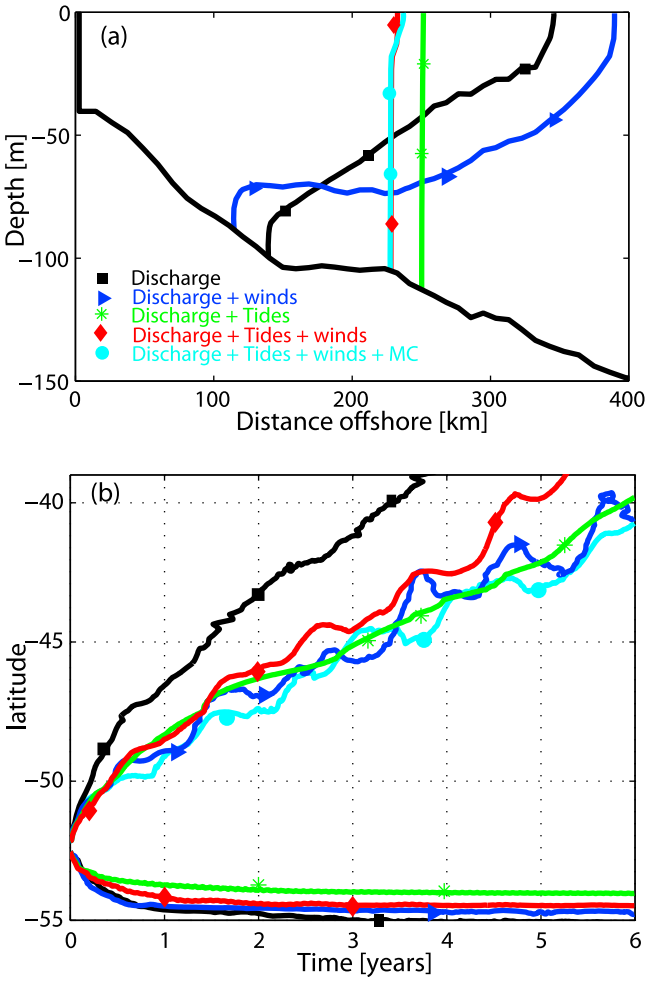

Figure 6. (a) Cross-shelf position of the 33.5 isohaline at Grande Bay section (CII, see Figure 1) for different forcing conditions. (b) Hovmöller diagrams of alongshore evolution of sea surface salinity minimum (only the 33.5 isohaline is depicted).

close to its observed position. This salinity front remains detached from the coast even after the MP waters leave the Grande Bay (Figure 7a).

[19] The observed offshore displacement of the MP front in EXP6 (Figure 7a) appears to be related to the "tidal diffusivity" mechanism postulated by *Ou et al.* [2003]. They argued that cross-shelf variations of tidal mixing leads to an offshore displacement of the maximum density gradient until it reaches twice the frictional depth (h_f), defined as

$$h_f = 2\sqrt{C_d U T}, \tag{2}$$

where Cd is the bottom friction coefficient ($\sim 2 \times 10^{-3}$) and U is the magnitude of the cross-shelf transport tidal-driven transport. Equation (2) is derived from *Okubo*'s [1967] estimate of the frictional depth and *Zimmerman*'s [1986] vertical diffusivity parameterization. Note that this estimate of the frictional depth has square-root dependence with the averaged velocity instead of the cubic dependence proposed by *Simpson and Hunter* [1974]. *Ou et al.* [2003] noted that the Simpson/Hunter estimate is strictly valid for summer fronts (what they called Type I fronts), but that vertically homogeneous fronts (Type II) are set by a different dynamical balance and hence have a different dependence of the depth-averaged velocity.

[20] Ou's theory on the offshore displacement of the salinity front appears to be pertinent to our results because the MP fulfills the two main conditions requested by the theory, first, that the plume be vertically homogenous (Figure 7b) and, second, that tidal currents in the region be very intense and strongly polarized in the cross-shelf direction [e.g., see *Glorioso and Flather*, 1997, Figure 3]. To assess Ou's theory we computed the depth-average cross-shore speeds at Grande Bay (Figure 8a, full line) and estimated an average cross-shelf transport (across the broken line marked in Figure 8a) of $U \sim 33.0$ [m^2/s]. Using this value and a period $T = 12.42$ h, equation (2) indicates that the maximum salinity gradient should be located at a depth $h \sim 105$ m, which is close to the location of the maximum salinity gradient in the model (Figure 8b).

[21] The inclusion of tidal forcing in EXP6 arrests the upstream spreading of the MP, a phenomenon similar to what is observed in the Chesapeake Bay [*Guo and Valle-Levinson*, 2007]. To identify the dynamical mechanisms responsible for the arresting process we did a new experiment, EXP6b (Table 1) that is similar to EXP6 but that was initialized it with the results of EXP4. At the steady state the surface salinity diminishes in Station P1 (see Figure 7a for the station location) and increases farther upstream (Station P2). The freshening at P1 is associated with the upstream advance of the plume, while the salinification at P2 is associated with a southward advection of saltier waters from the middle and outer shelf (Figure 7a). Tidally induced advection also leads to the separation of the MP from the coast at the San Jorge Gulf. The time evolution at station Q1 shows a salinity increase that is associated with the onshore advection of saltier waters from the outer shelf (Figure 7a). The freshening at station Q2 is related with the continuous northeastward advection of fresher waters from the inflow. Thus, tidal residual currents generate a circulation pattern that arrests the upstream development of the MP and forces its detachment from the coast.

[22] EXP7 adds tides and wind-forcing to the EXP4 (Table 1 and Figure 9). The overall structure of the plume in this experiment resembles EXP6 (tides only) (Figure 7), but shows an increase of the downstream and upstream extensions of the plume and a decrease of its cross-shelf extent. Thus, the new plume is narrower and more elongated. The downstream extension of the MP is driven by a strengthening of the northeastward flow (Figure 9b), while the upstream extension is driven by a geostrophic current flowing poleward along the coast (Figure 9c) [*Palma et al.*, 2004b]. The narrowing of the MP is associated with the strengthening of the along-shelf mean flow; this strengthening is driven by the wind-forcing [e.g., *Chapman and Lentz*, 1994]. The increase of the mean flow can be better appreciated in the comparison of the downstream sections of the along-shelf velocity fields of EXP6 and EXP7 and its corresponding northward volume transport (Figures 7c and 9b).

[23] To further quantify the impact of different forcings on the buoyancy transports we computed the normalized, annually averaged, buoyancy transport (Q_b/Q_{bi}) at two cross-shelf sections extending from the coast to the 33.5 isohaline.

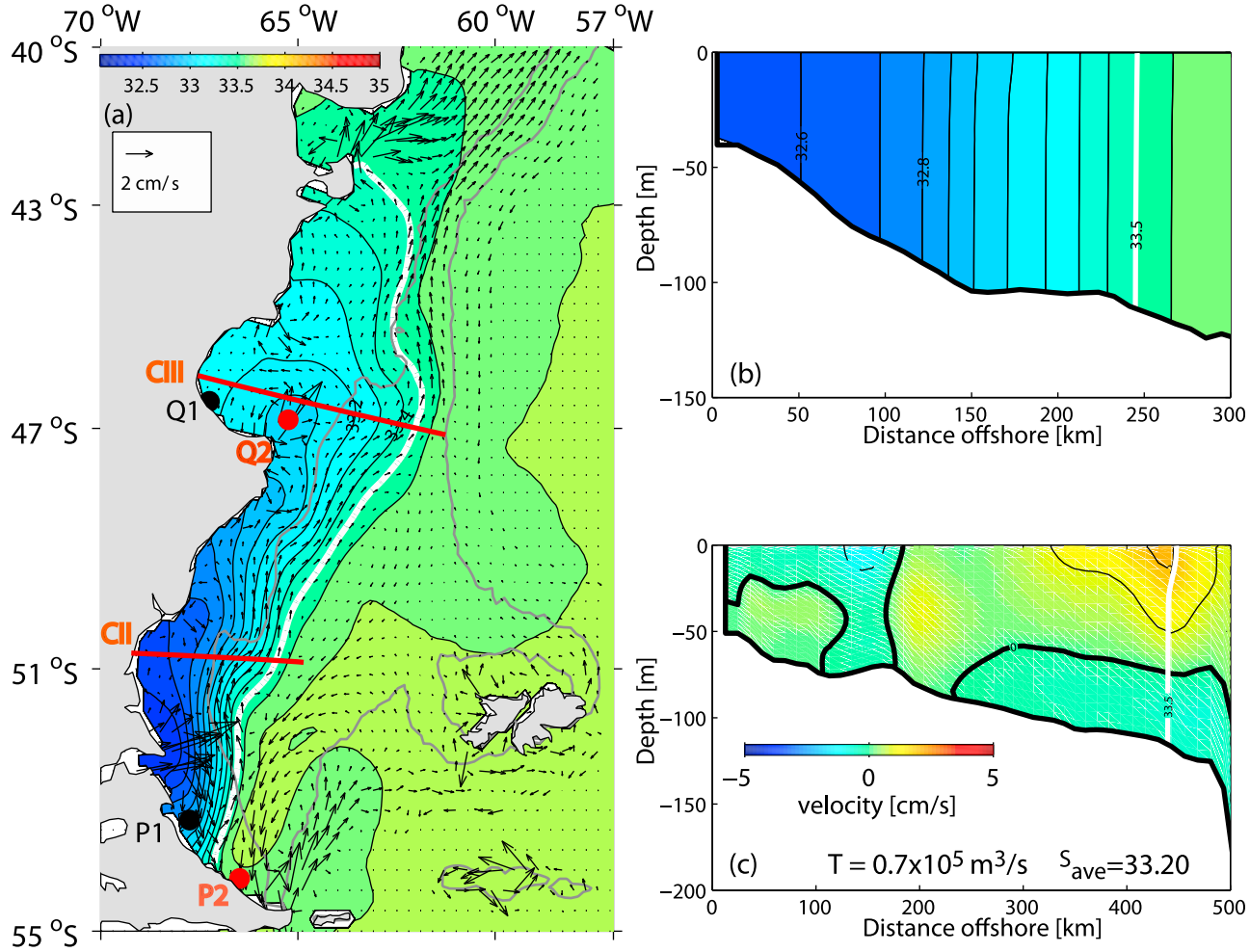

Figure 7. (a) Sea surface salinity and depth-averaged velocity vectors in the Patagonian Shelf from the experiment forced by the discharge and tides (EXP6). (b) Cross section of salinity at section CII. (c) Cross-section of along-shelf velocity at section CIII. The white line indicates the 33.5 isohaline. The volume transport through the section (limited offshore by this isohaline) and the area averaged salinity are also indicated.

The downstream increase of the buoyancy transport of EXP7 is similar to the transport of EXP4 (unforced) but larger than those of EXP5 (wind-forcing) and EXP6 (tidal forcing) (Table 2). The observed increment in EXP7 is produced by the wind-driven intensification of the northward transport, which is 2.5 times larger than in EXP6. The increase of the upstream transport in EXP7 is associated with the strengthening of the southward coastal current, which advects lighter waters upstream (e.g., Figure 9c).

[24] EXP8 was designed to assess the impact of the MC on the structure of the MP. To avoid inconsistencies between the initial and the boundary conditions, this experiment was initialized with the salinity structure derived from the World Ocean Atlas climatology (see *Palma et al.* [2008] for a detailed description of the model setup). To avoid the bias introduced by the salinity signature of the plume in the initial conditions we replaced salinities smaller than 33.7 with 33.7. The modified salinity field was then smoothed using a four-point Laplacian operator. EXP8 was started from rest and run during three years with only the boundary forcing, i.e., the MC. After that we included the buoyancy discharge, the tides and the wind-forcing (monthly climatological winds) and ran the experiment for another six years. The analysis is based on the averages of the last year of integration.

[25] EXP8 shows a retraction of the offshore and along-shelf extension of the MP. The cross-shore retraction is associated with the intensification of the along-shelf mean flow (Figure 10a), which is driven by the barotropic pressure gradient generated by the MC [*Palma et al.*, 2008]. The upstream buoyancy transport of EXP8 is nearly identical to that of EXP7, but the downstream transport is reduced to approximately 60% of its former value (Table 2). This reduction is caused by the shrinking of the cross-sectional area of the plume (limited offshore by the 33.5 isohaline) and the increase of the average salinity, which is associated with the onshore entrainment of saltier waters from the MC (Figure 10b).

[26] The plume in EXP8 spreads far beyond the observed limit of the MP, which is located near the Valdés Peninsula (~42°S). In fact, none of our previous experiments has been able to stop the spreading of the simulated MP at this

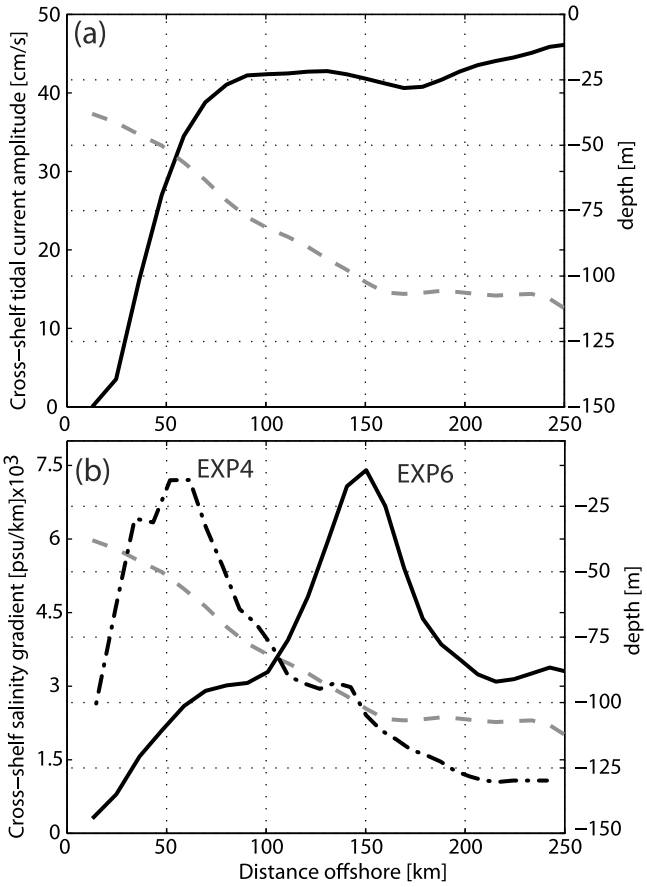

Figure 8. (a) M_2 cross-shelf tidal current amplitude at Grande Bay section (CII). (b) Cross-shelf salinity gradient for EXP6 (full black line) and EXP4 (dashed-dotted line). The gray broken line in both figures indicates the depth distribution.

location. This indicates that the northern limit of the MP could be set by the outflow of saltier waters from the San Matías Gulf, which is a highly evaporative region located at 41°30′S (Figure 1) [*Scasso and Piola*, 1988; *Lucas et al.*, 2005]. To test this hypothesis we ran EXP9, which was initialized from the results of EXP8 but included a relaxation of the surface salinity to a value of S = 34 within the San Matias Gulf (a reasonable approximation to the average salinity of this region). EXP9 produces an outflow of saltier waters from the San Matias Gulf into the open shelf that arrests the northward spreading of the MP. After a one year integration the MP limit retracts to its observed location (Figure 11b). There is a clear correlation between the negative (i.e., saltier) buoyancy outflow from the San Matias Gulf and the surface salinity increase farther south (Figures 11c and 11d). This confirms that the northward limit of the MP is set by the high salinity outflow from the San Matias Gulf.

4.4. Sensitivity Experiments

[27] To test the sensitivity of the previous experiments to variations in the forcing we did an additional set of experiments varying the magnitude of the wind stress forcing and the magnitude (Q_o) and salinity anomaly (ΔS) of the Magellan discharge. For the purposes of comparison we will use EXP9, which is our most realistic experiment, as a benchmark.

4.4.1. Sensitivity to Wind Intensity

[28] To test the plume's sensitivity to the wind-forcing we did experiments doubling (EXP10) and halving the wind intensity (EXP11). These experiments show that the northward limit of the plume is not very sensitive to the wind intensity but the eastward limit is (Figures 12a and 12d). In EXP10 the eastward limit of the plume expands south of 50°S and contracts farther north. The southward expansion is driven by the increase of the offshore (wind-driven) currents (e.g., Figure 12b). The northward retraction of the MP is driven by the onshore advection of saltier waters from the outer shelf (Figure 12c), which reduces the downstream buoyancy transport by approximately 10% (Table 2). The increase of the wind strength also produces intensification of the geostrophic currents in the southern portion of the Grande Bay (Figure 12c) and a threefold increment of the upstream buoyancy transport (Table 2). Halving the wind intensity has the opposite effect and the buoyancy transport increases in the downstream region and decreases upstream (Figures 12e and 12f and Table 2).

4.4.2. Sensitivity to the Magnitude and Salinity of the Discharge

[29] The buoyancy flux (Q_{bi}) of the Magellan discharge is a function of the volume of the discharge (Q_o) and of the salinity anomaly (ΔS) (equation (1)). To test the sensitivity of the MP to variations of these parameters we did four additional experiments. The first two, EXP12 and EXP13, have the same salinity anomaly as the benchmark experiment but in EXP12 the discharge is doubled (Q_o = 170,000 m^3/s) and in EXP13 the discharge is halved (Q_o = 42,500 m^3/s). The MP is very sensitive to the volume of the discharge. In EXP12, the increase of the discharge leads to an increase of the buoyancy transport and an increase of the downstream penetration of the MP (Table 2 and Figure 13a). Conversely, in EXP13 the weakening of the discharge decreases the downstream buoyancy transport and the northward penetration of the plume (Table 2 and Figure 13b). These experiments show that the magnitude of the normalized upstream buoyancy transport is inversely proportional to the volume flux of the discharge. This is in agreement with previous results showing that the downstream spreading of a plume is driven by the barotropic pressure gradient associated with the magnitude of the discharge, while the upstream spreading is forced by the baroclinic pressure gradient associated with the salinity anomaly of the discharge [*Matano and Palma*, 2010a]. A decrease of the discharge reduces the barotropic pressure gradient and hence the downstream spreading of the plume. This, in turn, leads to a larger upstream advance of the plume (e.g., Table 2). Experiments maintaining the benchmark's discharge magnitude (Q_o = 85000 m^3/s) and modifying the salinity anomaly in such a way as to keep the same buoyancy input as in EXP12 and EXP13 produce almost identical results.

4.5. Buoyancy Effects on the Shelf Mean Circulation and Transport

[30] To quantify the dynamical impact of the Magellan discharge on the shelf circulation, we computed the differences between the depth-averaged velocities of the benchmark experiment (EXP9) and the experiment without the Magellan discharge (EXP14, Table 1). The Magellan discharge generates a northward flowing current with maximum

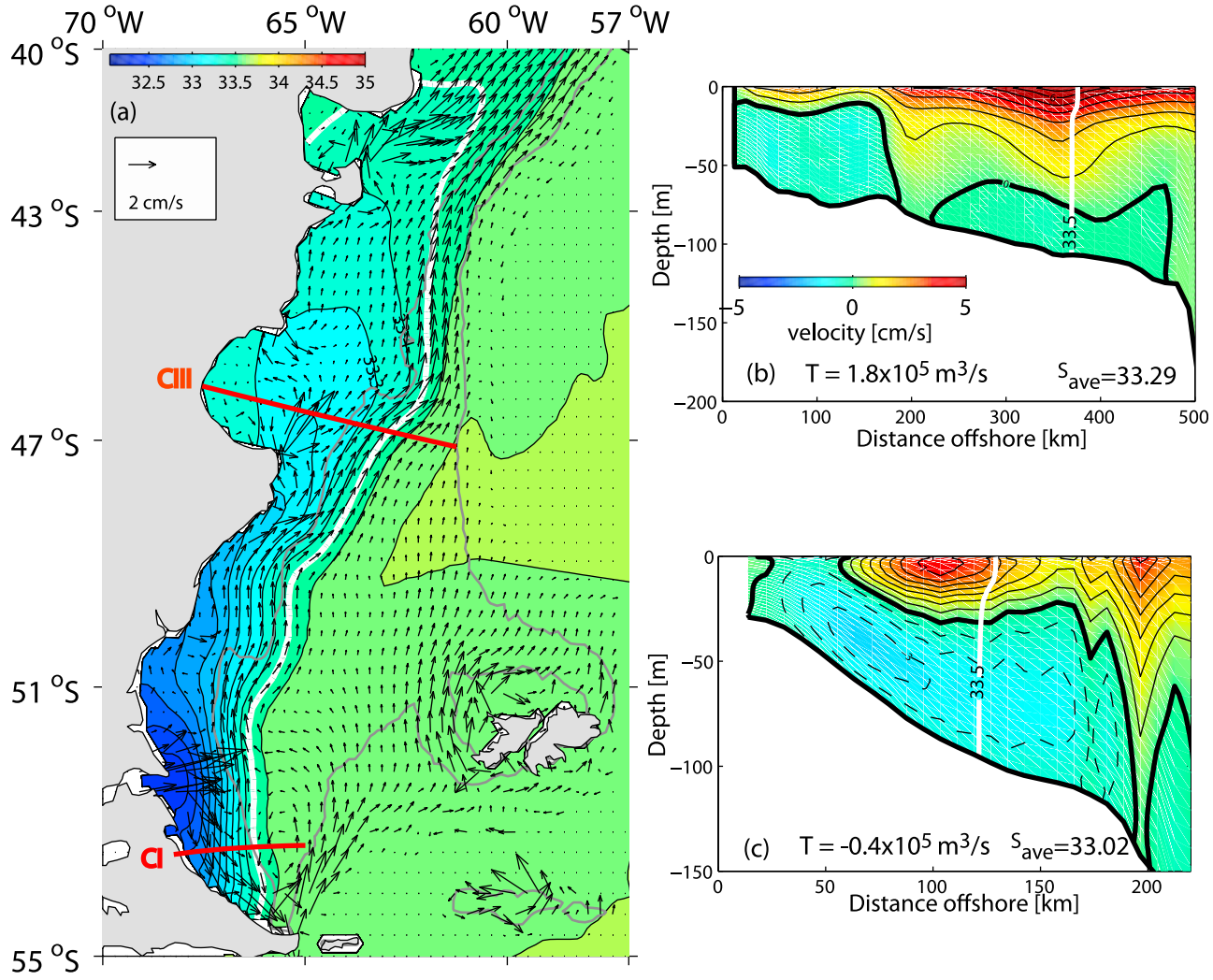

Figure 9. (a) Sea surface salinity and depth-averaged velocity vectors in the Patagonian Shelf from the experiment forced by the discharge, tides and winds (EXP7). (b) Cross-section of along-shelf velocity at section CIII. (c) Same as Figure 9b but for section CI. The white line indicates the 33.5 isohaline. The northward volume transport through the sections (limited offshore by this isohaline) and the area averaged salinity are also indicated.

speeds in the middle shelf (near the 100 m isobath) that extends from 53°S to 41°S (Figure 14c). This current has an average speed of approximately 1 cm/s and a volume transport of ~0.15 Sv. South of ~51°S the interaction between the buoyancy driven pressure gradients and the wind stress forcing increases the volume transport of southward flowing depth-averaged currents. The MP affects the overall structure of the depth-averaged currents in southern Patagonia. For

Table 2. Normalized Buoyancy Transport Through Cross-Sections CI and CIII[a]

	Year 1		Year 2		Year 3		Year 4		Year 5		Year 6	
Experiment	CI	CIII	CI	CIII	CI	CIII	CI	CIII	CI	CIII	CI	CIII
EXP4	−0.11	0.00	−0.12	0.33	−0.13	0.53	−0.11	0.64	−0.12	0.69	−0.14	0.70
EXP5	−0.07	0.00	0.04	0.00	0.05	0.22	0.05	0.31	0.06	0.38	0.07	0.50
EXP6	0.01	0.00	0.00	0.00	−0.04	0.25	−0.08	0.32	−0.09	0.31	−0.11	0.31
EXP7	−0.09	0.00	−0.27	0.00	−0.30	0.45	−0.35	0.64	−0.34	0.69	−0.36	0.71
EXP8	−0.09	0.00	−0.22	0.00	−0.27	0.29	−0.32	0.35	−0.32	0.41	−0.33	0.42
EXP10	−0.19	0.00	−0.39	0.00	−0.50	0.00	−0.54	0.35	−0.57	0.33	−0.58	0.36
EXP11	−0.06	0.00	−0.17	0.00	−0.22	0.26	−0.23	0.41	−0.23	0.46	−0.23	0.47
EXP12	−0.09	0.00	−0.19	0.27	−0.22	0.53	−0.23	0.62	−0.23	0.64	−0.24	0.63
EXP13	−0.11	0.00	−0.28	0.00	−0.37	0.00	−0.42	0.00	−0.43	0.00	−0.44	0.21

[a]See Figure 9. For EXP5 the buoyancy transport at CIII needs 10 years to reach a steady state.

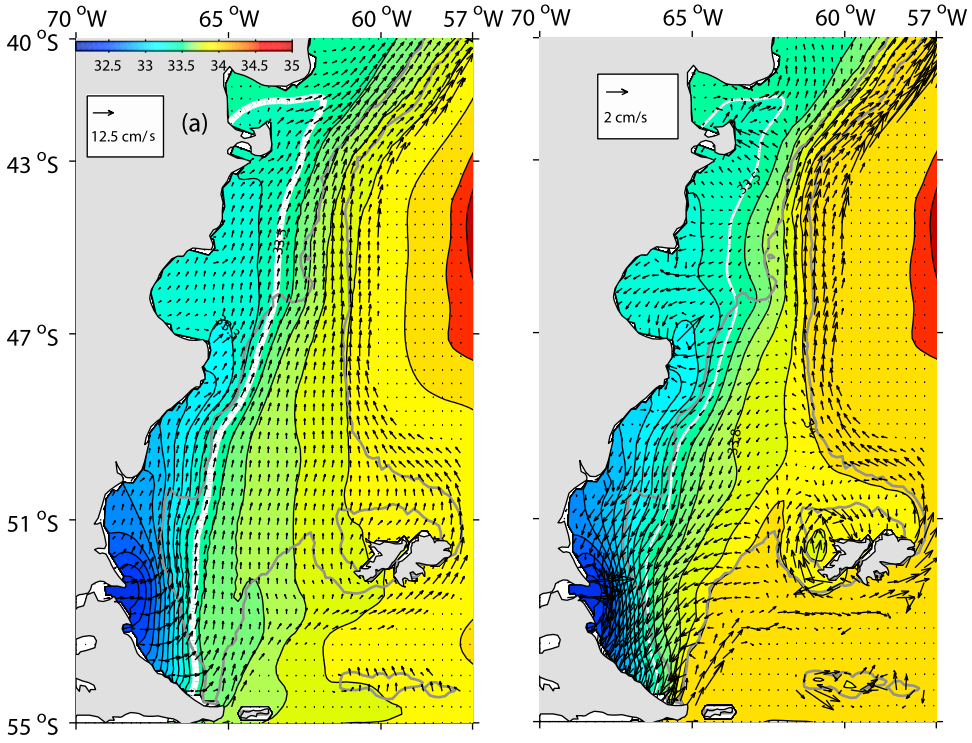

Figure 10. (a) Sea surface salinity and surface layer velocity vectors in the Patagonian Shelf from the experiment forced by the discharge, tides, winds and the MC (EXP8). (b) Bottom layer salinity and bottom layer velocity vectors.

example, the Grande Bay gyre, which is clearly shown in Figure 14a and in previous barotropic simulations [*Glorioso and Flather*, 1995; *Palma et al.*, 2004b] (see also Figure 2b) is split into a southward gyre with increased coastal currents and a region of weak currents north of the strait (Figure 14b).

5. Discussion and Conclusions

[31] The MP has several remarkable characteristics, some are associated with the environment in which it flows and some with its own structure. The environmental conditions includes an exceptionally large volume discharge, large tidal amplitudes, strong wind stress forcing, and the proximity to one of the world's largest western boundary currents. Given this unique combination of factors it is unsurprising that the salinity structure of the MP shows an array of remarkable characteristics. First, its unusual areal coverage which extends ~1800 km in the along-shelf direction while reaching to depths of more than 100 m. Second, its unusual trajectory which does not follow the coastline, as it would be expected from a typical buoyant plume, but instead flows along the 100 m isobath. In this study we have attempted to explain some of these characteristics.

[32] Our study indicates that the structure of the MP is primarily shaped by tidal effects, which manifests through tidal mixing and tidal residual currents. Strong vertical mixing associated to large tidal amplitudes homogenizes the MP vertically and keep it as a bottom-trapped plume against other forcing factors (e.g., winds). The spatial inhomogeneity in the tidal mixing associated with strong cross-shore motions appears to drive the offshore displacement of the plume front at Grande Bay [*Ou et al.*, 2003]. The analytical model of Ou et al. appears to be particularly relevant to this region because the MP plume is vertically homogeneous, and the region has large M_2 currents that are strongly polarized in the cross-shelf direction. However, although the predicted location of the front based on this theory agrees reasonable well with our numerical results there are obvious limitations of the proposed theory (a two-dimensional model) and the computation of the cross-shelf volume transport. Our three-dimensional model includes realistic coastline and topography and other physical processes not considered in Ou's theory (e.g., residual currents), which might contribute to sharpen the local gradients. The circulation pattern generated by the tidal residual currents also affects the along-shelf plume structure. In southern Grande Bay, the advection of saltier (offshore) waters arrests the upstream spreading of the plume while north of 47°S it forces the plume detachment off the coast producing a middle shelf low-salinity core.

[33] The MP is also strongly influenced by the wind-forcing. Away from the coast, the wind stress forcing creates a cross-shelf recirculation that increases the stratification of the water column and forces a detachment of the plume from the bottom. When the wind is combined with tidal forcing, however, the strong and persistent mixing restricts this effect to a very shallow surface layer and maintains the plume attached to the bottom. The synergetic interaction of tidal and wind-forcing reinforces the downstream and upstream buoyancy transports of the plume. The increase of the downstream transport is driven by the tidal homogenization and the wind-driven enhancement of the northward

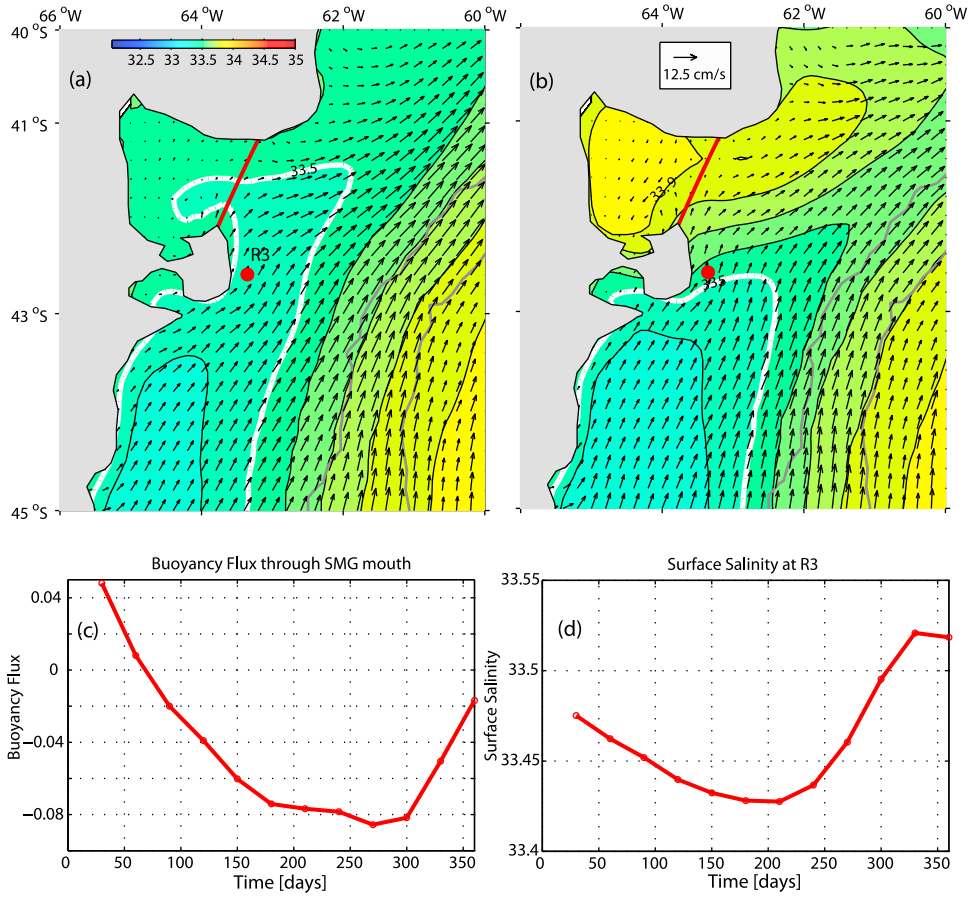

Figure 11. (a) Sea surface salinity and surface layer velocity vectors in the Patagonian Shelf from the experiment forced by the discharge, tides, winds and the Malvinas Current (EXP9). (b) Same as Figure 11a but with a surface relaxation toward SSS = 34 in San Matias Gulf (SMG). (c) Time evolution of buoyancy flux through SMG mouth (indicated in red in Figures 11a and 11b). (d) Time evolution of SSS at point R3.

transport. The increase of the upstream transport is driven by the strengthening of a geostrophically balanced coastal current that augments the southward transport. When the wind intensifies, the eastward limit of the plume expands south of 50°S but contracts farther north. The expansion is driven by the increase of the offshore (wind-driven) surface currents while the retraction is a consequence of a larger onshore advection of saltier waters from the outer shelf. A reduction of the wind intensity has the opposite effect. Variations in wind strength also make substantial modifications in the buoyancy fluxes generated by the Magellan discharge with a weakening (strengthening) in downstream fluxes and intensification (reduction) of upstream fluxes for stronger (weaker) winds (Table 2). An additional effect on the propagation of the MP is brought by the presence of an intense offshore boundary current. It has been shown that the MC has more influence on the shelf north of 50°S, where there is an intensification of the along-shelf mean flow driven by cross-shelf barotropic pressure gradients and onshore entrainment of denser oceanic waters [*Palma et al.*, 2008]. The overall effect on the downstream portion of the MP is a shrinking of the plume's cross-sectional area and a substantial reduction in the downstream buoyancy transport (Table 2). Finally, our experiments also indicate that the northward limit of the plume is set by the discharge of saltier waters from the San Matias Gulf. Without this outflow the MP would extend up to the La Plata River (~35°S).

[34] While the focus of our research has been the MP, some of the experimental results presented herein are of broader concern. For example, our experiments including only the discharge (EXP4) highlight the importance of along-shelf changes of bottom topography on the plume structure, spreading rate and buoyancy fluxes distribution. The MP cross-shelf width is larger at Grande Bay, shrinks near Cape Blanco and expands again after 47°S. These changes are inversely proportional to the bottom topography and are in accordance with the seminal results of *Chapman and Lentz* [1994]. The along-shelf variations in bottom slope also modify the downstream spreading rate of the plume; it moves faster in higher slopes and decreases in speed in gentler slopes in agreement with the idealized model of *Matano and Palma* [2010a]. The buoyancy transport partition is also related to the bottom slope; gentler slopes (i.e., Grande Bay) enhance the downstream transport and reduce the upstream contribution. This phenomenon is the subject of current research.

[35] The MP is very sensitive to the volume transport. The increase of the discharge leads to an increase of the

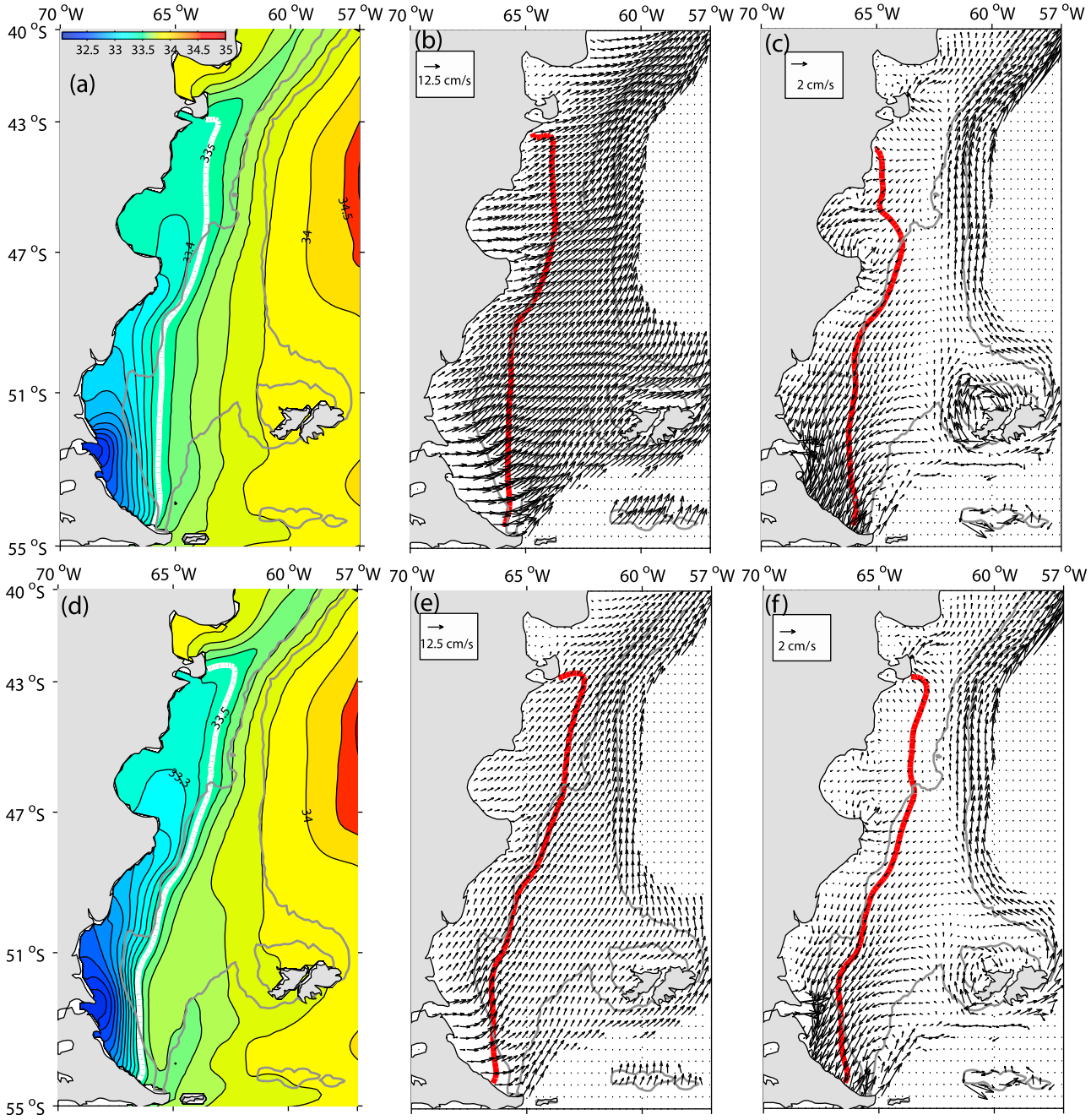

Figure 12. (a) Sea surface salinity, (b) surface layer velocity vectors and (c) bottom velocity vectors in the Patagonian Shelf from the experiment doubling the wind intensity. The red line indicates de position of the 33.5 isohaline. (d) SSS, (e) surface layer velocity vectors and (f) bottom velocity vectors from the experiment halving the wind intensity.

downstream penetration and buoyancy transport of the MP. Conversely, the weakening of the discharge decreases the buoyancy transport and the northward penetration of the plume. Furthermore the magnitude of the normalized *upstream* buoyancy transport is inversely proportional to the volume flux of the discharge. This behavior of the MP is consistent with our previous studies on idealized plumes [*Matano and Palma*, 2010a, 2010b] and illustrates the different role played by the barotropic and baroclinic pressure gradient in the dynamics of bottom-trapped plumes. The downstream spreading of a plume is driven by the barotropic pressure gradient associated with the magnitude of the discharge, while the upstream spreading is forced by the baroclinic pressure gradient associated with the salinity anomaly of the discharge. A decrease of the discharge reduces the barotropic pressure gradient and hence the downstream spreading of the plume. This, in turn, leads to a larger upstream advance of the plume.

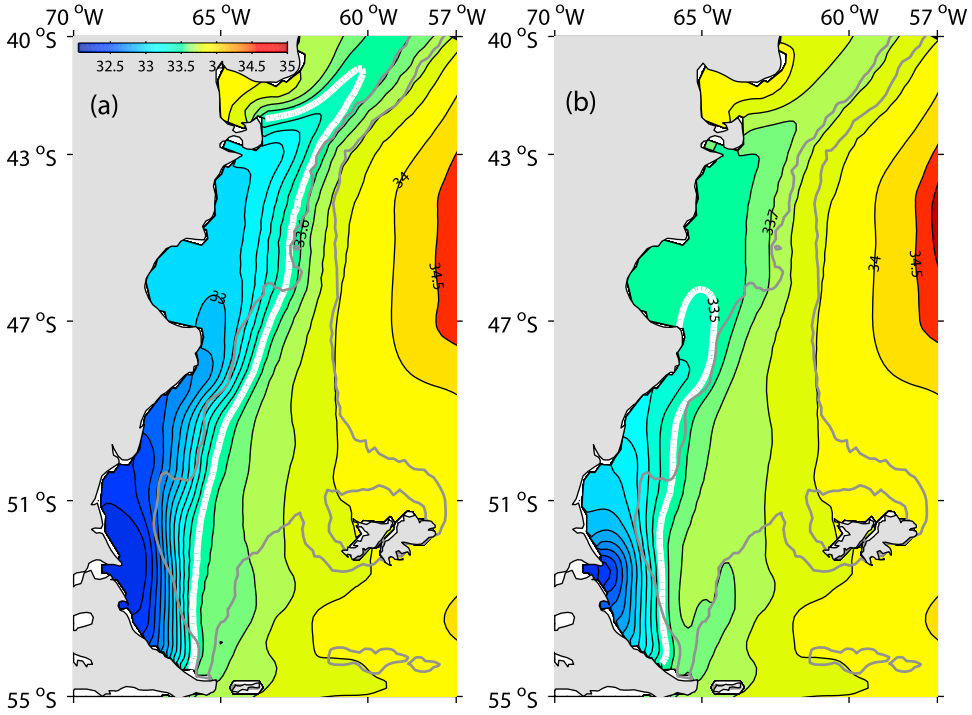

Figure 13. Sea surface salinity in the Patagonian Shelf from the sensitivity experiments: (a) doubling the Magellan discharge Q = 170,000 m^3/s and (b) halving the discharge Q = 42,500 m^3/s.

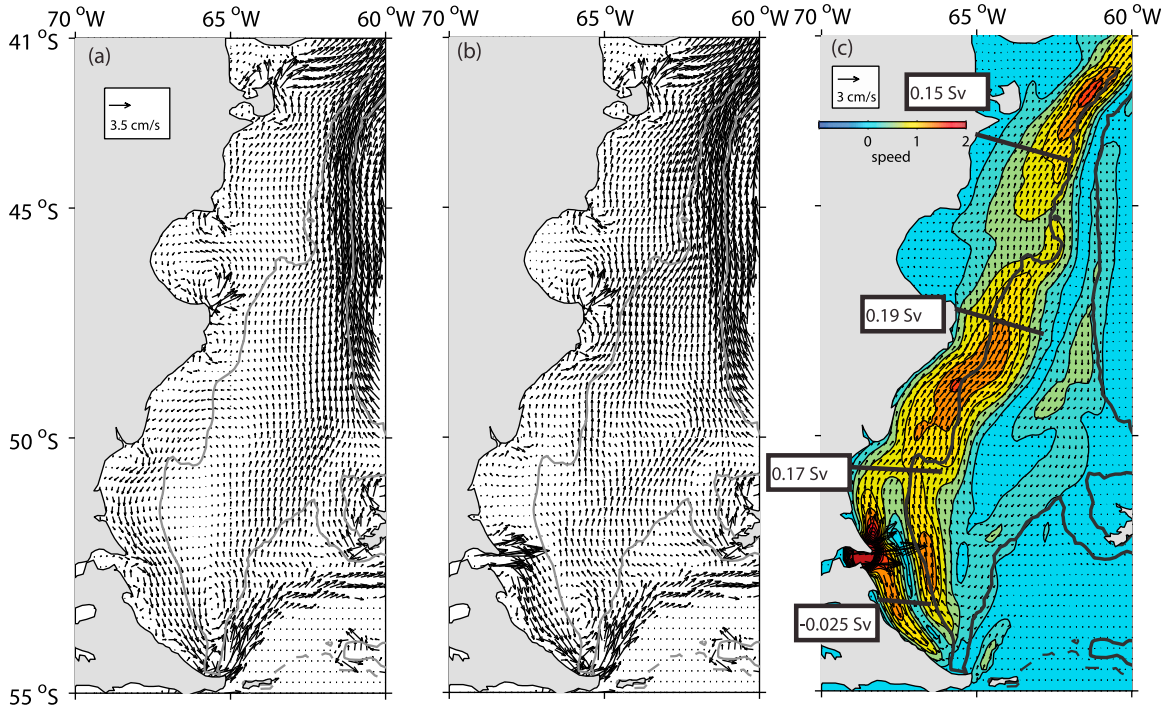

Figure 14. Depth averaged velocity vectors in the Patagonian Shelf, (a) EXP14 (full forcing without Magellan inflow, (b) EXP9 (full forcing with Magellan inflow) and (c) difference between Figures 14a and 14b. Colors indicate current intensity and numbers inside boxes the northward transport through the selected cross-sections. Gray lines indicate the 100 and 200 m isobaths.

[36] It has long been speculated that associated with the MP there is a northeastward current called the Patagonian Current [*Brandhorst and Castello*, 1971]. Although there are still few current meter observations to confirm this hypothesis our numerical simulations show that the Magellan Strait's discharge generates a relatively weak (∼1.0 cm/s) northeastward current in the middle shelf (roughly following the 100 m isobaths) that extends from 53°S to 41°S and promotes a northward transport of ∼0.15 Sv. Additionally, the MS discharge also modified the average circulation in the Grande Bay, the simulation without the discharge show the generation of a large anticyclonic gyre that covers a large part of the Grande Bay. The formation of this gyre has been reported in previous numerical studies with barotropic forcing [*Glorioso and Flather*, 1995; *Palma et al.*, 2004b]. The inclusion of the MS discharge modifies the overall horizontal structure of the depth-averaged circulation in this area, generating a smaller southern recirculating gyre with increased coastal currents and a region of weaker currents north of the strait.

[37] **Acknowledgments.** This article has strongly benefited from the comments and suggestions of three anonymous reviewers. The authors would also like to acknowledge Alberto Piola for kindly providing the data used to construct Figure 1 and for several useful discussions concerning the dynamics of the Magellan Plume. E. D Palma acknowledges the financial support from CONICET (PIP09-112-200801), Agencia Nacional de Promoción Científica y Tecnológica (PICT08–1874), Universidad Nacional del Sur (24F044), MINCyT/CONAE (001) and additional support from the Inter-American Institute for Global Change Research (IAI) CRN 2076 which is supported by the U.S. National Science Foundation (GEO-0452325). R. P. Matano acknowledges the financial support of the National Science Foundation through grant OCE-0928348, and NASA through grants NNX12AF67G and NNX08AR40G.

References

Bianchi, A. A., L. Bianucci, A. R. Piola, D. R. Pino, I. Schloss, A. Poisson, and C. F. Balestrini (2005), Vertical stratification and air-sea CO_2 fluxes in the Patagonian shelf, *J. Geophys. Res.*, *110*, C07003, doi:10.1029/2004JC002488.

Blumberg, A. F., and G. L. Mellor (1987), A description of a three-dimensional coastal ocean circulation model, in *Three-Dimensional Coastal Ocean Models*, *Coastal Estuarine Sci.*, vol. 4, edited by N. S. Heaps, pp. 1–16, AGU, Washington, D. C., doi:10.1029/CO004p0001.

Brandhorst, W., and J. P. Castello (1971), Evaluación de los recursos de anchoita (Engraulis Anchoita) frente a la Argentina y Uruguay. Parte I. Las condiciones oceanográficas, sinopsis del conocimiento actual sobre la anchoita y el plan para su evaluación, *Proy. Des. Pesq. Ser. Inf. Tec.*, *29*, 1–63.

Chapman, D. C., and S. J. Lentz (1994), Trapping of a coastal density front by the bottom boundary layer, *J. Phys. Oceanogr.*, *24*, 1464–1479, doi:10.1175/1520-0485(1994)024<1464:TOACDF>2.0.CO;2.

Csanady, G. T. (1978), The arrested topographic wave, *J. Phys. Oceanogr.*, *8*, 47–62, doi:10.1175/1520-0485(1978)008<0047:TATW>2.0.CO;2.

Egbert, G. D., A. F. Bennet, and M. G. G. Foreman (1994), TOPEX/POSEIDON tides estimated using a global inverse model, *J. Geophys. Res.*, *99*, 24,821–24,852, doi:10.1029/94JC01894.

Fong, D. A., and W. R. Geyer (2002), The alongshore transport of freshwater in a surface-trapped river plume, *J. Phys. Oceanogr.*, *32*, 957–972, doi:10.1175/1520-0485(2002)032<0957:TATOFI>2.0.CO;2.

Galperin, B., L. Kantha, S. Hassid, and A. Rosati (1988), A quasi-equilibrium turbulent energy model for geophysical flows, *J. Atmos. Sci.*, *45*, 55–62, doi:10.1175/1520-0469(1988)045<0055:AQETEM>2.0.CO;2.

Glorioso, P. D., and R. A. Flather (1995), A barotropic model of the currents off SE South America, *J. Geophys. Res.*, *100*, 13,427–13,440, doi:10.1029/95JC00942.

Glorioso, P. D., and R. A. Flather (1997), The Patagonian Shelf tides, *Prog. Oceanogr.*, *40*, 263–283, doi:10.1016/S0079-6611(98)00004-4.

Guo, X., and A. Valle-Levinson (2007), Tidal effects on estuarine circulation and outflow plume in the Chesapeake Bay, *Cont. Shelf Res.*, *27*, 20–42, doi:10.1016/j.csr.2006.08.009.

Kourafalou, V., L. Oey, J. Wang, and T. Lee (1996), The fate of river discharge on the continental shelf: 1. Modelling the river plume and the inner shelf coastal current, *J. Geophys. Res.*, *101*, 3415–3434, doi:10.1029/95JC03024.

Lucas, A. J., R. A. Guerrero, H. W. Mianzan, E. M. Acha, and C. A. Lasta (2005), Coastal oceanographic regimes of the Northern Argentine Continental Shelf (34–43°S), *Estuarine Coastal Shelf Sci.*, *65*, 405–420, doi:10.1016/j.ecss.2005.06.015.

Matano, R. P., and E. D. Palma (2010a), The upstream spreading of bottom-trapped plumes, *J. Phys. Oceanogr.*, *40*, 1631–1650, doi:10.1175/2010JPO4351.1.

Matano, R. P., and E. D. Palma (2010b), The spindown of bottom-trapped plumes, *J. Phys. Oceanogr.*, *40*, 1651–1658, doi:10.1175/2010JPO4352.1.

Matano, R. P., E. D. Palma, and A. R. Piola (2010), The influence of the Brazil and Malvinas Currents on the southwestern Atlantic shelf circulation, *Ocean Sci.*, *7*, 837–871, doi:10.5194/osd-7-837-2010.

Mellor, G. L., and T. Yamada (1982), Development of a turbulence closure model for geophysical fluid problems, *Rev. Geophys.*, *20*, 851–875, doi:10.1029/RG020i004p00851.

Okubo, A. (1967), The effect of shear in an oscillatory current on horizontal diffusion from an instantaneous source, *Int. J. Oceanol. Limnol.*, *1*, 194–204.

Ou, H. W., C. M. Dong, and D. Chen (2003), Tidal diffusivity: A mechanism for frontogenesis, *J. Phys. Oceanogr.*, *33*, 840–847, doi:10.1175/1520-0485(2003)33<840:TDAMFF>2.0.CO;2.

Palma, E. D., R. P. Matano, A. R. Piola, and L. Sitz (2004a), A comparison of the circulation patterns over the Southwestern Atlantic driven by different wind stress climatologies, *Geophys. Res. Lett.*, *31*, L24303, doi:10.1029/2004GL021068.

Palma, E. D., R. P. Matano, and A. R. Piola (2004b), A numerical study of the Southwestern Atlantic Shelf circulation: Barotropic response to tidal and wind forcing, *J. Geophys. Res.*, *109*, C08014, doi:10.1029/2004JC002315.

Palma, E. D., R. P. Matano, and A. R. Piola (2008), A numerical study of the Southwestern Atlantic Shelf circulation: Stratified ocean response to local and offshore forcing, *J. Geophys. Res.*, *113*, C11010, doi:10.1029/2007JC004720.

Panella, S., A. Michelato, R. Perdicaro, G. Magazzu, F. Decembrini, and P. Scarazzato (1991), A preliminary contribution to the understanding of the hydrological characteristics of the Strait of Magellan: Austral spring 1989, *Boll. Oceanol. Teor. Appl.*, *9*(2–3), 106–126.

Pasquini, A. I., and P. J. Depetris (2007), Discharge trends and flow dynamics of South American rivers draining the southern Atlantic seaboard: An overview, *J. Hydrol.*, *333*(2–4), 385–399, doi:10.1016/j.jhydrol.2006.09.005.

Piola, A. R., S. I. Romero, and U. Zajaczkovski (2008), Space-time variability of the Plata plume inferred from ocean color, *Cont. Shelf Res.*, *28*, 1556–1567, doi:10.1016/j.csr.2007.02.013.

Piola, A. R., N. Martínez Avellaneda, R. A. Guerrero, F. P. Jardón, E. D. Palma, and S. I. Romero (2010), Malvinas-slope water intrusions on the northern Patagonia continental shelf, *Ocean Sci.*, *6*, 345–359, doi:10.5194/os-6-345-2010.

Ridderinkhof, H. (1989), Tidal and residual flows in the western Dutch Wadden Sea III: Vorticity balances, *Neth. J. Sea Res.*, *24*, 9–26, doi:10.1016/0077-7579(89)90166-X.

Risien, C. M., and D. B. Chelton (2008), A global climatology of surface wind and wind stress fields from eight years of QuikSCAT scatterometer data, *J. Phys. Oceanogr.*, *38*, 2379–2413, doi:10.1175/2008JPO3881.1.

Robinson, I. S. (1983), Tidally induced residual flow, in *Physical Oceanography of Coastal and Shelf Seas*, *Elsevier Oceanogr. Ser.*, vol. 35, edited by B. Johns, pp. 321–356, Elsevier, Amsterdam.

Romero, S. I., A. R. Piola, M. Charo, and C. A. E. Garcia (2006), Chlorophyll-a variability off Patagonia based on SeaWiFS data, *J. Geophys. Res.*, *111*, C05021, doi:10.1029/2005JC003244.

Sassi, M. G., and E. D. Palma (2006), Modelo hidrodinámico del estrecho de Magallanes, *Mec. Comput.*, *XXV*(16), 1461–1479.

Scasso, L. M. L., and A. R. Piola (1988), Intercambio neto de agua entre el mar y la atmósfera en el Golfo San Matías, *Geoacta*, *15*, 13–31.

Simpson, J. H., and J. R. Hunter (1974), Fronts in the Irish Sea, *Nature*, *250*, 404–406, doi:10.1038/250404a0.

Smagorinsky, J. (1963), General circulation experiments with the primitive equations: Part I. The basic experiment, *Mon. Weather Rev.*, *91*(3), 99–164, doi:10.1175/1520-0493(1963)091<0099:GCEWTP>2.3.CO;2.

Smith, R. D., and D. T. Sandwell (1997), Global sea floor topography from satellite altimetry and ship depth soundings, *Science*, *277*, 1956–1962, doi:10.1126/science.277.5334.1956.

Smolarkiewicz, P. K., and W. W. Grabowski (1990), The multidimensional positive definite advection transport algorithm, *J. Comput. Phys.*, *86*, 355–375, doi:10.1016/0021-9991(90)90105-A.

Tokmakian, R., and P. G. Challenor (1999), On the joint estimation of model and satellite sea surface height anomaly errors, *Ocean Modell.*, *1*, 39–52.

Vivier, F., and C. Provost (1999), Volume transport of the Malvinas Current: Can the flow be monitored by TOPEX/POSEIDON?, *J. Geophys. Res.*, *104*(C9), 21,105–21,122, doi:10.1029/1999JC900056.

Wu, H., J. Zhu, J. Shen, and H. Wang (2011), Tidal modulation of the Cangjiang River plume in summer, *J. Geophys. Res.*, *116*, C08017, doi:10.1029/2011JC007209.

Yankovsky, A. E., and D. C. Chapman (1997), A simple theory for the fate of coastal discharges, *J. Phys. Oceanogr.*, *27*, 1386–1401, doi:10.1175/1520-0485(1997)027<1386:ASTFTF>2.0.CO;2.

Zimmerman, J. T. F. (1986), The tidal whirlpool: A review of horizontal dispersion by tidal and residual currents, *Neth. J. Sea Res.*, *20*, 133–154, doi:10.1016/0077-7579(86)90037-2.